Solution of the Onsager model for the structure of rigid rods confined on a spherical surface

Wu-Yang Zhang, Ying Jiang, and Jeff Z. Y. Chen
Guelph-Waterloo Physics Institute and Department of Physics and Astronomy, University of Waterloo, Waterloo N2L 3G1, Ontario, Canada
(Received 30 March 2012; published 28 June 2012)

We consider a free energy, within the framework of the Onsager approximation, for a spatially and orientationally inhomogeneous distribution of hard rods confined on a spherical surface. These rods interact with each other though the excluded-volume interaction, forming a textured nematic structure on the spherical surface at high surface coverage. Our numerical solution to the model shows that the splay state, where on average rods line up in parallel to the longitudes on the spherical surface, is the only stable state. Other types of textures that have recently been suggested were also tested and all yield higher free energy than that of a ground splay state. We also provide a study of the disorder-splay transition, which is shown to have first-order characteristics.

DOI: 10.1103/PhysRevE.85.061710 PACS number(s): 61.30.Cz, 64.70.M−, 61.30.Hn

I. INTRODUCTION

A nematic liquid confined on a closed surface forms a spatially inhomogeneous nematic director field. At a theoretical level, the interest in the coupled positional and orientational ordering can find a root in understanding the so-called hairy-ball theorem—accompanying a vector field on the smooth, closed surface are always some field singularities. The Poincaré-Hopf theorem of differential geometry states that the sum of indexes of all the topological defects must equal the Euler characteristic of the closed surface—two for a spherical surface.

Consistent with this expectation, Nelson [1] suggested the possibility of creating a four-fold tetravalent colloid particle by coating it with a nematic shell, a sheet of anisotropic objects such as nanorods, polymers, or gemini lipids. In this case, the micron-sized particles would have four chemical linkers similar to sp^3 hybridized chemical bonds of carbon, silicon, and germanium atoms and then are able to arrange into a colloidal crystal with a diamond structure. Liquid-crystal experiments have displayed the existence of these structures [2,3], and proposals have been made to exploit these interesting properties in materials [4–7].

The conformation consisting of Mermin's boojums [8]—the so-called splay conformation [Fig. 1(a_I)]—is normally thought of as the configuration for the nematic shell confined to a spherical surface in a high density. The structure contains two $+1$ defects at the north and south poles and is consistent with the Poincaré-Hopf theorem. The possibility of the four-fold tetrahedral symmetry of a nematic shell confined on a spherical surface [Fig. 1(a_{II})] has been predicted by phenomenological theories, such as the Frank continuum theory [1,9,10] and the Landau-de Gennes model [11,12]. Such a tennis-ball conformation contains four $+1/2$ defects appearing at the vertices of an equally sided tetrahedron on the spherical surface [1,9].

A good theoretical example of such a nematic field is the one generated by rigid rods at high densities, confined on a sphere of radius R. Generally, in a rod-on-surface model, the system consists of N rodlike particles of length L, which interact with each other through an excluded-volume interaction. The orientational and positional entropies dominate at a low surface rod coverage, giving rise to a system in an isotropic state with no particular structural ordering. As the surface density goes beyond a transition density, a nematic field starts to develop in the system. An interesting question then becomes the following: what type of defect configurations would this system display? In this paper we focus on this well-defined model system which contains no phenomenological constants assumed in previous studies [1,9,11,12].

The competition between the entropic effects and the excluded-volume interaction can be transparently reflected by the main ingredients in an Onsager theory [13], which has been used for describing nematic structure of rigid rods in three dimensions [14]. In this work we generalize the free-energy expression of Onsager, now suitable for a spatially inhomogeneous system on a spherical surface, to study the resulting nematic defect structure. As explained in our preliminary report [15] and further detailed in this paper, the only stable state we obtained was the splay configuration, within the considered parameter range. This agrees with the observation of recent Monte Carlo simulations of *thin* rods confined on a spherical surface [16,17]. The result also agrees with the general Frank-energy theory—rod systems have $K_1 \ll K_3$ [18,19], hence they only display the splay configuration [1].

Then, what drives the stability of the experimentally observed nonsplay structures? Liquid-crystal molecules, which are not exactly rigid, contain some semiflexibility. An interesting real system is the liquid of 5CB molecules, which has $K_1 \approx K_3$ [20]. This falls into the range of Frank constants where the tennis-ball structure can be stable. Indeed, a double emulsion experiment indicates assorted defect structures in a thin layer of 5CB liquid crystals [3].

Based on a Monte Carlo snapshot of rods on a spherical surface, Bates [17] suggested a structure where the vector joining the two defects near the north pole is parallel to the vector joining the other pair near the south pole [17]. The defects show up at the four corners of a flat rectangle, intersecting a great circle [(Fig. 1(a_{III})]. By means of computer simulations, Shin *et al.* [16] and Bates [17] also suggested the existence of another interesting state that was called a "cut-and-rotate" splay configuration—the pattern resembles cutting a perfect splay state along the north-south pole plan and then rotating one of the hemispheres by an angle [Fig. 1(a_{IV})]. We will assess the Onsager free energies of these possible configurations in this paper to evaluate their instability.

We aim at finding an exact solution of the free-energy model [Sec. II A] using a multiple-variable approach [Sec. II C], so that the free energy can be minimized with no ambiguous

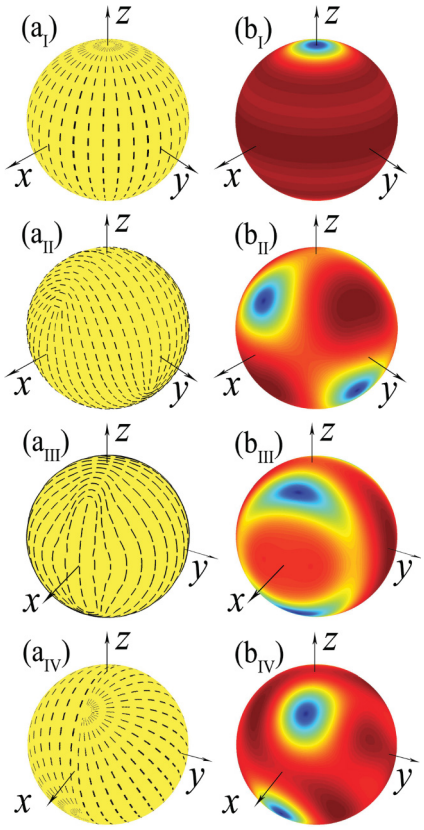

FIG. 1. (Color online) Four possible configurations considered in this work: ($a_{\rm I}$) and ($b_{\rm I}$) splay, ($a_{\rm II}$) and ($b_{\rm II}$) tennis-ball, ($a_{\rm III}$) and ($b_{\rm III}$) rectangle, and ($a_{\rm IV}$) and ($b_{\rm IV}$) cut-and-rotate splay. Plots ($b_{\rm I}$)–($b_{\rm IV}$) represent entropy field maps that are produced according to the procedure explained in Sec. III D, from our numerical solution in this work.

approximations. Incorporating the symmetric properties of the splay, tennis-ball, rectangle, and cut-and-rotate splay configurations [Sec. II B], we can also enforce the system to search for the possible existence of these different states. One of the main results from this exercise is that the global minimum of the free energy corresponds to only one state, namely, the splay state. Within a wide range of the searched parameter space, tennis-ball, rectangle, and cut-and-rotate splay configurations do not correspond to a free-energy minimum [Secs. III A–III D]. Furthermore we defined the orientational and positional order parameters that can be used to characterize the physical properties near the disorder-splay transition point [Sec. III E] and found that the nature of the transition is first order, within the current mean-field approach [Sec. III F]. Some results in this paper were reported earlier [15].

II. MODEL

A. Free-energy functional

We consider a system of N rigid "rods" which are embedded on the surface of a sphere of radius R. Because straight rods cannot be completely confined on a curved surface, here we use the model that each rod is a curved geodesic segment of length L, which is a portion of the so-called great circle. These rod particles interact with each other through the excluded-volume interaction. Note that on a two-dimensional surface the excluded volume actually manifests itself into the form of an excluded area, which always exists even at an extremely small, vanishing rod radius to length ratio. In this work we assume that rods have no thickness D, which can be considered as an approximation for actual systems having small D/L.

In his classical work [13], Onsager developed a free-energy functional for the three-dimensional, spatially homogeneous system of rigid rods interacting with each other through the excluded-volume interaction, as a functional of the density distribution. We can easily generalize his approach to write down the free energy of the current system, now including both spatial and orientational dependencies:

$$\beta F = \int \varrho(\mathbf{r},\mathbf{u}) \ln[8\pi^2 R^2 \varrho(\mathbf{r},\mathbf{u})]\, d\mathbf{r}d\mathbf{u} + \frac{1}{2}\int \varrho(\mathbf{r},\mathbf{u}) w(\mathbf{r},\mathbf{u},\mathbf{r}',\mathbf{u}') \varrho(\mathbf{r}',\mathbf{u}')\, d\mathbf{r}d\mathbf{u}d\mathbf{r}'d\mathbf{u}'. \quad (1)$$

In the above, we have assumed a density distribution function $\varrho(\mathbf{r},\mathbf{u})$, where $\mathbf{r}$ and $\mathbf{u}$ are the position vector and tangent unit vector, respectively, of the center of mass of a rod. The first term arises from both orientational and translational entropies, where a linear term $\varrho(\mathbf{r},\mathbf{u}) \ln 8\pi^2 R^2$ has been added which does not affect the structure of the current theory. The second term contains a function $w(\mathbf{r},\mathbf{u},\mathbf{r}',\mathbf{u}')$ that depends on variables $(\mathbf{r},\mathbf{u})$ and $(\mathbf{r}',\mathbf{u}')$, which represent the coordinates of the centers of mass of two rods; this function takes a value of 1 if any parts of the two rods overlap and 0 otherwise. Although only accurate at the level of the second-virial approximation, the competition between the entropy and the excluded-volume terms captures the important physics in most systems involving rigid rods, such as the isotropic-nematic liquid-crystal phase transition [13,21], the isotropic-nematic interface [22–28], and nematic rods near a hard wall surface [29–31].

To proceed further we adopt a spherical-coordinate system to specify the position of the center of mass of a rod by the polar and azimuthal variables Θ and Φ, shown in Fig. 2. The orientation of a rod is described by θ, the angle that $\mathbf{u}$ makes with respect to the longitude passing through the center of mass. The density distribution function $\varrho(\Theta,\Phi;\theta)$ satisfies

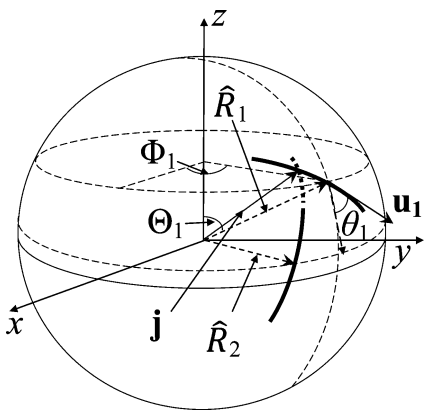

FIG. 2. Coordinate system used in this work. The location of a rod is specified by the polar angle Θ and azimuthal angle Φ, and the orientation of the rod is specified by the angle between the tangent vector $\mathbf{u}$ and the local longitude.

the normalization condition

$$R^2 \int \varrho(\Theta,\Phi;\theta)\sin\Theta d\Theta d\Phi d\theta = N, \tag{2}$$

where N is the total number of rods in the system. Furthermore, we introduce the probability distribution function

$$f(\Theta,\Phi;\theta) \equiv R^2\varrho(\Theta,\Phi;\theta)/N, \tag{3}$$

which can be interpreted as the probability for finding the center of mass of a rod at the position described by (Θ,Φ) and with an orientation represented by θ. The function $f(\Theta,\Phi;\theta)$ is now normalized to

$$\int f(\Theta,\Phi;\theta)\sin\Theta d\Theta d\Phi d\theta = 1. \tag{4}$$

As a functional of the probability distribution function $f(\Theta,\Phi;\theta)$, the free energy can be rewritten as

$$\begin{aligned}\beta F = {} & N\ln N + N\int f(\Theta,\Phi;\theta)\ln[8\pi^2 f(\Theta,\Phi;\theta)] \\ & \times \sin\Theta d\Theta d\Phi d\theta + \frac{N^2}{2}\int f(\Theta,\Phi;\theta) \\ & \times w(\Theta,\Phi,\theta,\Theta',\Phi',\theta') f(\Theta',\Phi';\theta') \\ & \times \sin\Theta\sin\Theta' d\Theta d\Phi d\theta d\Theta' d\Phi' d\theta'. \end{aligned} \tag{5}$$

The equilibrium state of the model can be found from a minimization of F with respect to $f(\Theta,\Phi;\theta)$.

The function $w(\Theta_1,\Phi_1,\theta_1,\Theta_2,\Phi_2,\theta_2)$ contains six variables and can be defined by using basic relations between the variables associated with two interacting rods. The orientation vector $\mathbf{u}_i$ and center-of-mass vector $\mathbf{r}_i$ of rod i, where $i = 1$ and 2, can be written as $\mathbf{u}_i = \cos\theta_i\hat{\Theta}_i + \sin\theta_i\hat{\Phi}_i$ and $\mathbf{r}_i = R\hat{R}_i$, where $\hat{R}$, $\hat{\Theta}$, and $\hat{\Phi}$ are unit vectors of the spherical-coordinate system. In this way we can define the normal to the great-circle plane for a particle located at $\mathbf{r}_i$, $\mathbf{n}_i = \mathbf{r}_i \times \mathbf{u}_i$. The direction from the sphere's center to the intersection point of two great circles on the sphere's surface is a vector that can be represented by $\mathbf{j} = \mathbf{n}_1 \times \mathbf{n}_2/|\mathbf{n}_1 \times \mathbf{n}_2|$, as illustrated in Fig. 2. Based on this vector relationship, the function w can be easily accessed:

$$w(\Theta_1,\Phi_1,\theta_1,\Theta_2,\Phi_2,\theta_2) = \begin{cases} 1, & \text{if } \mathbf{j}\cdot\hat{R}_i > \cos(L/2R) \\ & \text{for both } i = 1 \text{ and } 2, \\ 1, & \text{if } \mathbf{j}\cdot\hat{R}_i < -\cos(L/2R) \\ & \text{for both } i = 1 \text{ and } 2, \\ 0, & \text{otherwise.} \end{cases} \tag{6}$$

The above is a function of L/R only for geodesic rods considered here. The leading correction for rods of finite D/L can also be written in a similar expression, but we focus on the case of $D/L = 0$ in the current work.

B. Symmetry properties

In this paper, we are mainly concerned about four possible configurations of the model system—splay, tennis-ball, rectangle, and cut-and-rotate splay. The density distribution functions for these four configurations carry unique symmetry properties, which are listed in Table I. The considered symmetry operations are

$$f(\Theta,\Phi;\theta) = f(\Theta,\Phi;\theta+\pi), \tag{7}$$

$$f(\Theta,\Phi;\theta) = f(\Theta,\Phi+\pi;\theta), \tag{8}$$

$$f(\Theta,\Phi;\theta) = f(\Theta,-\Phi;-\theta), \tag{9}$$

$$f(\Theta,\Phi;\theta) = f(\pi-\Theta,\Phi+\pi/2;\pi-\theta), \tag{10}$$

$$f(\Theta,\Phi;\theta) = f(\pi-\Theta,\Phi;\pi-\theta), \tag{11}$$

$$f(\Theta,\Phi;\theta) = f(\pi-\Theta,\pi-\Phi;\pi+\theta), \tag{12}$$

$$\partial f(\Theta,\Phi;\theta)/\partial\Phi = 0. \tag{13}$$

Below we find useful representations of the symmetries that define these configurations and simplify the numerical procedure accordingly.

C. Numerical approach

In order to minimize the free energy, computationally we could represent the function in question, $f(\Theta,\Phi;\theta)$, by direct discretization of all three involved variables. Such discretization was considered previously for similar rod systems where two or three variables were involved [26,27]. Because of the large number of independent parameters needed to numerically represent $f(\Theta,\Phi;\theta)$ in high precision, other numerical tricks were required. In this work we decided to take an expansion of $f(\Theta,\Phi;\theta)$ in terms of orthonormal basis functions, adjusting expansion coefficients to minimize the free energy.

The basis functions,

$$\psi_{lmn}(\Theta,\Phi;\theta) = Y_{lm}(\Theta,\Phi)U_n(\theta), \tag{14}$$

TABLE I. Symmetry properties of the distribution functions of the four considered configurations.

Configuration	Eq. (7)	Eq. (8)	Eq. (9)	Eq. (10)	Eq. (11)	Eq. (12)	Eq. (13)
Splay	√	√	√	√	√	√	√
Tennis-ball	√	√	√	√			
Rectangle	√	√	√		√		
Cut-and-rotate splay	√	√				√	

are a combination of the spherical harmonics $Y_{lm}(\Theta,\Phi)$ and Fourier bases $U_n(\theta)$. We adopt the real version:

$$Y_{lm}(\Theta,\Phi)=\begin{cases}\sqrt{2}\sqrt{\frac{2l+1}{4\pi}\frac{(l-m)!}{(l+m)!}}P_l^m(\cos\Theta)\cos(m\Phi) & \text{if} \quad m>0,\\ \sqrt{\frac{2l+1}{4\pi}}P_l^0(\cos\Theta) & \text{if} \quad m=0,\\ \sqrt{2}\sqrt{\frac{2l+1}{4\pi}\frac{(l+m)!}{(l-m)!}}P_l^{|m|}(\cos\Theta)\sin(|m|\Phi) & \text{if} \quad m<0,\end{cases} \tag{15a}$$

$$U_n(\theta)=\begin{cases}\frac{1}{\sqrt{\pi}}\cos(n\theta) & \text{if} \quad n>0,\\ \frac{1}{\sqrt{2\pi}} & \text{if} \quad n=0,\\ \frac{1}{\sqrt{\pi}}\sin(|n|\theta) & \text{if} \quad n<0,\end{cases} \tag{15b}$$

where P_l^m is the associate Legendre function of the lth and mth rank [32]. The basis functions follow

$$\int \psi_{lmn}(\Theta,\Phi;\theta)\psi_{l'm'n'}(\Theta,\Phi;\theta)\sin\Theta d\Theta d\Phi d\theta = \delta_{ll'}\delta_{mm'}\delta_{nn'}, \tag{16}$$

where δ_{ij} is the Kronecker delta.

The function w can be then expanded in terms of the orthonormal bases:

$$w(\Theta,\Phi,\theta,\Theta',\Phi',\theta') = \frac{L^2}{4\pi R^2}\sum_{lmn,l'm'n'}\psi_{lmn}(\Theta,\Phi;\theta)W_{lmn,l'm'n'} \times \psi_{l'm'n'}(\Theta',\Phi';\theta'). \tag{17}$$

At a given value of L/R, the constant matrix, $W_{lmn,l'm'n'}$, can be evaluated according to

$$W_{lmn,l'm'n'} = \frac{4\pi R^2}{L^2}\int \psi_{lmn}(\Theta,\Phi;\theta)w(\Theta,\Phi,\theta,\Theta',\Phi',\theta') \times \psi_{l'm'n'}(\Theta',\Phi';\theta')\sin\Theta\sin\Theta' d\Theta d\Phi d\theta d\Theta' d\Phi' d\theta'. \tag{18}$$

A constant, $4\pi R^2/L^2$, has been factored out in the above to properly account for the magnitude of the excluded volume. The integral part of Eq. (18) contains further L/R dependence through the expression in Eq. (6). In this work, numerically the integral was evaluated by means of Simpson's approximation [33], at an integration step $L/36R$ for Θ and Φ, as well as $\pi/36$ for θ; the results were stored as a constant matrix before further computation takes place.

The unknown function, f, can then be expressed in terms of unknown coefficients ϕ_{lmn} in the expansion

$$f(\Theta,\Phi;\theta)=\sum_{lmn}\phi_{lmn}\psi_{lmn}(\Theta,\Phi;\theta). \tag{19}$$

The normalization condition, Eq. (4), can be directly used to determine the coefficient of the leading basis function, labeled $(l,m,n)=(0,0,0)$:

$$\psi_{000}=1\big/\sqrt{8\pi^2}, \tag{20}$$

which gives

$$\phi_{000}=1\big/\sqrt{8\pi^2}. \tag{21}$$

The free energy can then be treated as a function of multiple variables, all ϕ_{lmn} other than ϕ_{000}, in our search for the free-energy minimum:

$$\beta F = N\ln N + N\int f(\Theta,\Phi;\theta)\ln[8\pi^2 f(\Theta,\Phi;\theta)] \times \sin\Theta d\Theta d\Phi d\theta + \frac{N^2L^2}{8\pi R^2}\sum_{lmn,l'm'n'}\phi_{lmn}W_{lmn,l'm'n'}\phi_{l'm'n'}. \tag{22}$$

The isotropic state is characterized by a constant density distribution. The expansions considered here yield a free energy for the isotropic state:

$$\beta F_0 = N\ln N + \frac{N^2L^2}{8\pi R^2}W_{000,000}\phi_{000}^2. \tag{23}$$

We can then write the reduced free-energy difference per particle:

$$\tilde{f} = (\beta F-\beta F_0)/N = \int f(\Theta,\Phi;\theta)\ln[8\pi^2 f(\Theta,\Phi;\theta)]\sin\Theta d\Theta d\Phi d\theta + \frac{\rho L^2}{2}{\sum_{lmn,l'm'n'}}'\phi_{lmn}W_{lmn,l'm'n'}\phi_{l'm'n'}, \tag{24}$$

where the summation $\sum'$ runs over all (l,m,n) and (l',m',n') except for the $(l,m,n)=(l',m',n')=(0,0,0)$ terms. Beyond ϕ_{lmn}, the system contains two parameters, the length/radius ratio L/R through the W matrix and the reduced density

$$\rho L^2 = \frac{NL^2}{4\pi R^2} \tag{25}$$

as the coefficient of the second term in Eq. (24). For each set of specified parameters, L/R and ρL^2, we attack the minimization problem, treating $\tilde{f}$ as a multivariable function of ϕ_{lmn}, where $(l,m,n)\neq(0,0,0)$.

In the actual computation, we took advantage of the symmetry properties listed in Sec. II B to reduce the number of unknown variables, ϕ_{lmn}. We approximated the expansion by neglecting terms having indexes $l=8$ $n=8$ and higher. This means that there are 16, 46, 49, and 91 bases needed to describe the splay, tennis-ball, rectangle, and cut-and-rotate splay configurations, respectively. The numerical error of ignoring higher-order terms is negligible, within the precision of required calculation.

The computational task for conducting the search of the free-energy minimum relied on an implementation of the Broyden-Fletcher-Goldfarb-Shanno (BFGS) algorithm explained in Ref. [34]. BFGS is a quasi-Newton method, which iteratively searches for a stationary point of a multivariable function starting from an initial guess. At each step, BFGS determines a search direction from the gradient and uses the approximation of the Hessian matrix to find the next point. The stationary point is considered stable until the mean-square magnitude of the gradient converges to a number less than a pre-specified tolerance. At every search step, the value of the

function to be minimized, Eq. (24), and its gradient,

$$G_{lmn} \equiv \frac{\partial \tilde{f}}{\partial \phi_{lmn}} = \int \{1 + \ln[8\pi^2 f(\Theta,\Phi;\theta)]\}\psi_{lmn}(\Theta,\Phi;\theta) \times \sin\Theta d\Theta d\Phi d\theta + \rho L^2 \sum_{l'm'n'} W_{lmn,l'm'n'}\phi_{l'm'n'}, \quad (26)$$

must be provided.

While the computational task of the W-related terms in both Eqs. (24) and (26) can be performed efficiently by taking summations, the integration in terms related to $\ln f(\Theta,\Phi;\theta)$ in both expressions is not straightforward and is most numerically expensive. For a given set ϕ_{lmn}, we evaluated the entire function $f(\Theta,\Phi;\theta)$ from the expansion, Eq. (19), and treated these integrations involving logarithmic terms taking a numerical integration based on Simpson's rule [33].

III. RESULTS AND DISCUSSION

A. Free-energy minimum

The model system that we are considering can be characterized by the length of the rod L, the radius of the confining sphere R, and the number of particles N. Out of these parameters, from a scaling point of view, only two reduced parameters are important, L/R, and the reduced surface density, ρL^2 in Eq. (25). Indeed, the reduced free energy, Eq. (24), contains these two reduced parameters only. The results discussed in this section are presented as a function of ρL^2, with selected L/R in the range [0.1,1].

As reported previously [15], within this range of L/R, from the current model we only found one type of ordered ground state, splay, regardless of various attempts in setting up an initial configuration that breaks the splay symmetry. The minimized splay free energies obtained from the numerical minimization for $L/R = 0.1$, 0.5, and 1 are displayed by solid curves in Fig. 3. The number of independent ϕ_{lmn} in the expansion Eq. (24) varies according to the underlying symmetry properties listed in Table I. Because the splay configuration has a higher symmetry than the other three, splay terms which exist in a splay configuration are also common in the expansions of the free energies for the other three types of configurations. For every given system, we have employed four different processes of conducting the minimization search. Each process corresponds to a study of a particular type of conformation; we directly search for the free-energy minimum of this conformation by varying the undetermined coefficients of all relevant terms and removing all other terms that violate the symmetry properties of such a state. By the end of the search, all four processes converge to one single result: ϕ_{lmn} of the splay terms are significantly present and ϕ_{lmn} of nonsplay terms vanish.

From the symmetry of the expansion, we see that every nonsplay configuration is characterized by a leading nonsplay term in the free-energy expansion, tennis-ball by the $(l,m,n) =$

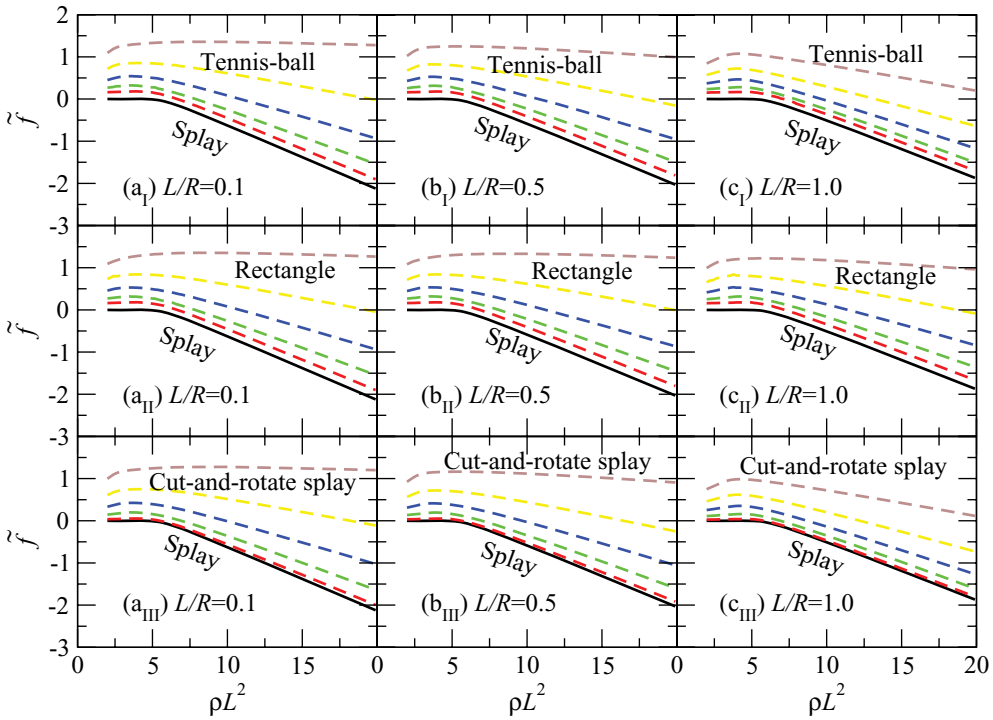

FIG. 3. (Color online) Minimized free energy plotted as a function of reduced density ρL^2 for (a) $L/R = 0.1$, (b) $L/R = 0.5$, and (c) $L/R = 1.0$. Plots (a_I), (b_I), and (c_I) show the free energies of the splay states (solid curve) and the tennis-ball states (dashed curves) with the leading term coefficient fixed at −0.1, −0.08, −0.06, −0.04, and −0.02, from the top to bottom curves. Plots (a_{II}), (b_{II}), and (c_{II}) show the free energies of the splay states (solid curve) and the rectangle states (dashed curves) with the leading term coefficient fixed at 0.1, 0.08, 0.06, 0.04, and 0.02, from the top to bottom curves. Plots (a_{III}), (b_{III}), and (c_{III}) show the free energies of the splay states (solid curve) and the cut-and-rotate splay states (dashed curves) with the leading term coefficient fixed at 0.1, 0.08, 0.06, 0.04, and 0.02, from the top to bottom curves.

(3,2,0) term, rectangle by (2,2,0), and cut-and-rotate splay by (3, − 2,0), as the result of the symmetry operation in Table I. In another analysis, we *fixed* one of these ϕ_{lmn} and numerically searched for the free-energy minima by varying other coefficients. The fixed ϕ_{lmn} was set at small increments, covering a significant range to ensure a thorough search. Examples of such a minimization procedure are displayed in Fig. 3 as well. The dashed curves in Figs. 3(a_I), 3(b_I), and 3(c_I) show the resulting free energies by keeping the tennis-ball order parameter $\phi_{3,2,0}$ fixed at −0.1, − 0.08, − 0.06, − 0.04, and −0.02, from the top to bottom. The dashed curves in Figs. 3(a_{II}), 3(b_{II}), and 3(c_{II}) show the resulting free energies by keeping the rectangle order parameter $\phi_{2,2,0}$ fixed at 0.1, 0.08, 0.06, 0.04, and 0.02, from the top to bottom. The dashed curves in Figs. 3(a_{III}), 3(b_{III}), and 3(c_{III}) show the resulting free energies by keeping the cut-and-rotate splay order parameter $\phi_{3,-2,0}$ fixed at 0.1, 0.08, 0.06, 0.04, and 0.02, from the top to bottom. Note the highest curves in all these plots have free energies far exceeding the free energy of the isotropic state (i.e., $\tilde{f}$ is significantly positive) at a wide range of ρL^2. Most importantly, $\tilde{f}$ as a function of ϕ_{lmn} for a considered ρL^2 changes monotonically. Within the parameter range searched in this work, we can rule out the existence of stable nonsplay configurations. As well, these plots demonstrate how other possible conformations converge to a splay ground state, as the relevant ϕ_{lmn} decreases.

B. Onsager model and the Frank energy

The coupled positional and orientational dependencies of the considered structure can be described by a nematic director field $\mathbf{n}(\mathbf{r})$; corresponding spatial derivatives $\nabla \cdot \mathbf{n}$, $\mathbf{n} \cdot (\nabla \times \mathbf{n})$, and $\mathbf{n} \times (\nabla \times \mathbf{n})$ characterize splay, twist, and bend distortions of the director field, respectively. The Frank elastic energy is written as a sum of quadratic powers of the derivatives, with the corresponding phenomenological splay, twist, and bend coefficients, K_1, K_2, and K_3 [35]. On a two-dimensional surface, $K_2 = 0$, and we are left with only splay and bend distortions,

$$F_{\text{Frank}} = \frac{1}{2}\int \left[K_1(\nabla \cdot \mathbf{n})^2 + K_3(\nabla \times \mathbf{n})^2\right] \sin\Theta d\Theta d\Phi. \tag{27}$$

For a nematic director field on a spherical surface, analysis showed [1,9,36] that the tennis-ball configuration has a lower elastic energy *if* the two coefficients have the same magnitude, $K_1 \sim K_3$.

The relationship between an Onsager model and the Frank energy was explored previously for nematic textures [18,37]. The basic idea in this comparison is to assume a distribution function $\varrho(\mathbf{r},\mathbf{u})$ in terms of $\mathbf{u}$ and $\mathbf{n}(\mathbf{r})$ and integrate out the $\mathbf{u}$ dependence so that the free energy is now dependent on $\mathbf{n}(\mathbf{r})$ only. As the next step, an expansion on $\mathbf{r}$, accurate to the square of the first-order derivatives, is carried out, leaving leading quadratic terms in the same structure as in the Frank energy. This way, one can pin down the Frank coefficients for nematic rods, without the phenomenological assumptions of the magnitude of K_1, K_2, and K_3. According to Refs. [18,19], such a comparison gives rise to $K_1 \simeq 0.06 \ll K_3 \simeq 0.4$ [18] in a system containing thin rods [16,17]. This estimate can be contrasted with the $K_1 \sim K_3$ requirement for the stabilization of a tennis-ball configuration discussed in Refs. [1,9] and is the reason why nematic, *rigid* rods do not display the tennis-ball configuration on a spherical surface. For the same reason, the rectangle configuration also requires a substantial component of bending of the overall texture and therefore is not preferred in a hard-rod system. Another related system, though theoretical, is a long self-avoiding semiflexible polymer chain confined on a spherical surface. Because of the flexibility along the chain, K_3 now becomes comparable to K_1. Using Monte Carlo simulations, our group recently concluded that this system displays a disorder-order transition, where the ordered state always accompanies the tennis-ball symmetry [38].

Monte Carlo simulations of nematic rods on a spherical surface agree with our results here [17]. It should be noted, however, that the analysis in Refs. [18,37] was conducted by assuming a specific distribution form in $\varrho(\mathbf{r},\mathbf{u})$ and was done in three-dimensional space. A similar analysis of K_1 and K_3 for nematic rods embedded on a curved surface would reveal the nature of the Frank constants further and would be useful.

C. Cut-and-rotate splay

In a Monte Carlo simulation, Shin *et al*. recently suggested the existence of the so-called cut-and-rotate splay conformation in closely packed hard rods [16], where $L/R \approx 0.4$ and $\rho L^2 \approx 14$. The hard rods were modeled by straight lines and confined to the tangent plane of the sphere, each rod having a nonzero diameter $D = L/15$. The excluded-volume interaction of this particular thickness-to-length ratio has the same effects as the excluded-area interaction of geodesic rods considered in this work. The cut-and-rotate splay configuration can be visualized as if it is made from a perfect splay by cutting the plane containing the north and south poles, rotating one of the hemispheres by an angle, and then reforming the structure by combining two hemispheres [Fig. 1(a_{IV})].

In the above we have already calculated the free energy of an enforced cut-and-rotate splay symmetry shown in Fig. 3, from a numerical solution of Eq. (24), by fixing a leading cut-and-rotate splay term, $\phi_{3,2,0}$. Here we take yet another approach to examine this state by actually exercising a "cut-and-rotate" process. We took the density distribution $f_{\text{spl}}(\Theta,\theta)$ of the splay conformation, which was obtained from the free-energy minimization, and cut it through the x-z plane. Then the distribution on the hemisphere containing the positive y axis was rotated by an $\alpha/2$ angle about the y axis, and the distribution on the other hemisphere is rotated by a $-\alpha/2$ angle. With the aid of the addition theorem of spherical harmonics, the new distribution could be easily obtained, which was substituted into Eq. (5) for evaluation of the free energy. In Fig. 4, we display the cut-and-rotate splay free energy per rod, as a function of the rotation angle α, for $L/R = 0.1$, 0.5, and 1.0. From the plots, we can see that the cut-and-rotate splay state always has a higher free energy in comparison with that of the splay state ($\alpha = 0$ or π). This is particularly so in large-L/R systems compared with small-L/R systems.

According to Shin *et al*., based on the Frank free-energy model, there is no free-energy cost for cutting and rotating [16]. This fact was used as a verification of their observations.

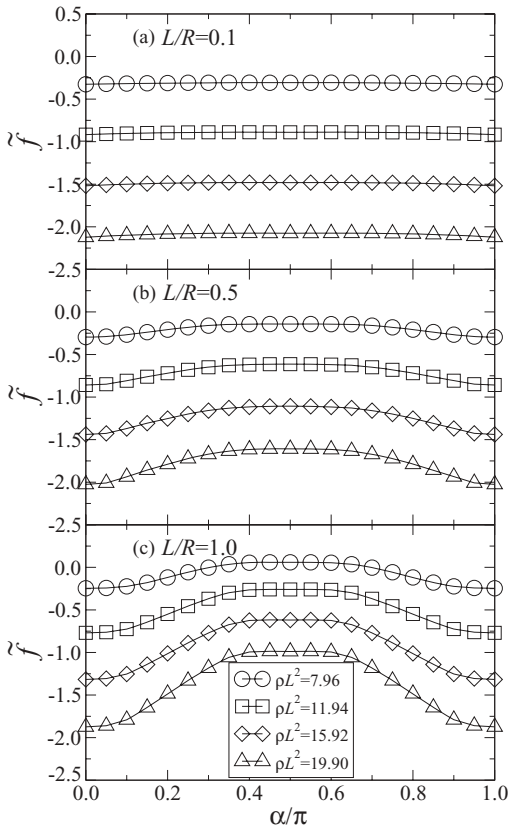

FIG. 4. Cut-and-rotate-splay free energy plotted as a function of the rotation angle α at various densities $\rho L^2 = 7.96$ (circles), 11.94 (squares), 15.92 (diamonds), and 19.90 (triangles) for (a) $L/R = 1.0$, (b) $L/R = 0.5$, and (c) $L/R = 1.0$, based on the solution of Eq. (5).

However, the angular distribution about the director field of this conformation contains a sharp change at the cutting circle. While the quadratic terms of the first derivative in Eq. (27) can be indeed recovered from the Onsager free energy, there are higher-order terms, both in higher powers of the first derivatives and higher-order derivatives of $\mathbf{n}(\mathbf{r})$. These higher-order derivatives, hence the unexpanded version of the Onsager free energy, disfavor such sharp changes by raising the free energy of the system. This effect rules out the cut-and-rotate splay in the current system.

The difference between the observation of Shin *et al*. and our results here remains unresolved. This could be attributed to the slow Monte Carlo dynamics normally seen in a highly packed system or the difference in the initial setups of these two studies.

D. Nematic director field, local entropy field, and defect visualization

As discussed above, all four possible configurations considered here contain coupled orientational and spatial ordering. In this subsection, we discuss an entropy field that can be defined from our numerical solution of the model in Eq. (5).

The left panels in Fig. 1 are idealized texture illustrations where the local nematic directors are indicated by *unit vectors* forming a director field. The important information on the local orientational entropy is not clearly represented in these plots. On the basis of the distribution function containing Θ, Φ, and θ as variables, here we consider a *scalar* orientational entropy field $\sigma(\Theta, \Phi)$, represented by a local orientational order parameter defined by the following procedure. First, a 2×2 matrix $\mathcal{S}$ was constructed:

$$\mathcal{S} = \langle 2\mathbf{uu} - \mathbf{I} \rangle = \begin{pmatrix} \langle \cos 2\theta \rangle & \langle \sin 2\theta \rangle \\ \langle \sin 2\theta \rangle & -\langle \cos 2\theta \rangle \end{pmatrix}. \tag{28}$$

The average $\langle \cdots \rangle$ is performed over the orientational distribution locally:

$$\langle \cos 2\theta \rangle = \frac{\int \cos 2\theta f(\Theta, \Phi; \theta) d\theta}{\int f(\Theta, \Phi; \theta) d\theta}, \tag{29a}$$

$$\langle \sin 2\theta \rangle = \frac{\int \sin 2\theta f(\Theta, \Phi; \theta) d\theta}{\int f(\Theta, \Phi; \theta) d\theta}. \tag{29b}$$

We then select the positive eigenvalue of the matrix $\mathcal{S}$ as a measure for the orientational entropy field:

$$\sigma(\Theta, \Phi) = \sqrt{\langle \cos 2\theta \rangle^2 + \langle \sin 2\theta \rangle^2}. \tag{30}$$

Figures 1(b_I)–1(b_{IV}) are illustrations of $\sigma(\Theta, \Phi)$ for $L/R = 0.5$ and $\rho L^2 = 12$, based on $f(\Theta, \Phi; \theta)$ determined from the present work, which was obtained for splay (all expansion coefficients free in minimization), tennis-ball ($\phi_{3,2,0}$ fixed at 0.1), rectangle ($\phi_{2,2,0}$ fixed at 0.1), and cut-and-rotate splay ($\phi_{3,-2,0}$ fixed at 0.1) configurations. A color scheme is used in the plot, where red, yellow, green, cyan, and blue are used to represent σ values ranging from high to low. These plots show that the structural defects can be visualized not only by the director field but also by an analysis of the orientational entropy field. In the splay configuration, two low-σ (high-entropy) defects are located at north and south poles. In a tennis-ball state, four low-σ defects occupy the vertices of a tetrahedron, which is a similar picture as the one displayed for the result of a Landau-de Gennes model under one-Frank constant approximation [12]. In a rectangle configuration, four low-σ defects can be seen along a great circle cutting through the x-z plane, where the pattern in a low-σ region is greatly distorted; in a cut-and-rotate splay configuration, four low-σ defects follow the same symmetry of the director-field defects; however, the locations of the lowest σ (off the x-z plane) do not completely overlap with the locations of the proposed defects (on the x-z plane) in the director field [16].

E. Splay order parameters

Next we examine two order parameters that characterize the overall orientational and positional ordering of the isotropic-splay phase transition. The global orientational order,

$$\Omega = \int \cos 2\theta f(\Theta, \Phi; \theta) \sin\Theta d\Theta d\Phi d\theta = 2\pi \phi_{002}, \tag{31}$$

yields a 0 value in the isotropic phase, a positive value in the splay phase where rods line up along the longitudes (observed here), and a negative value in the helicoidal phase where rods line up along the latitudes. The fact that we only see a positive Ω for *rigid* rods verifies $K_1 \ll K_3$ discussed in Sec. III B; this was noted by Nelson in Ref. [1].

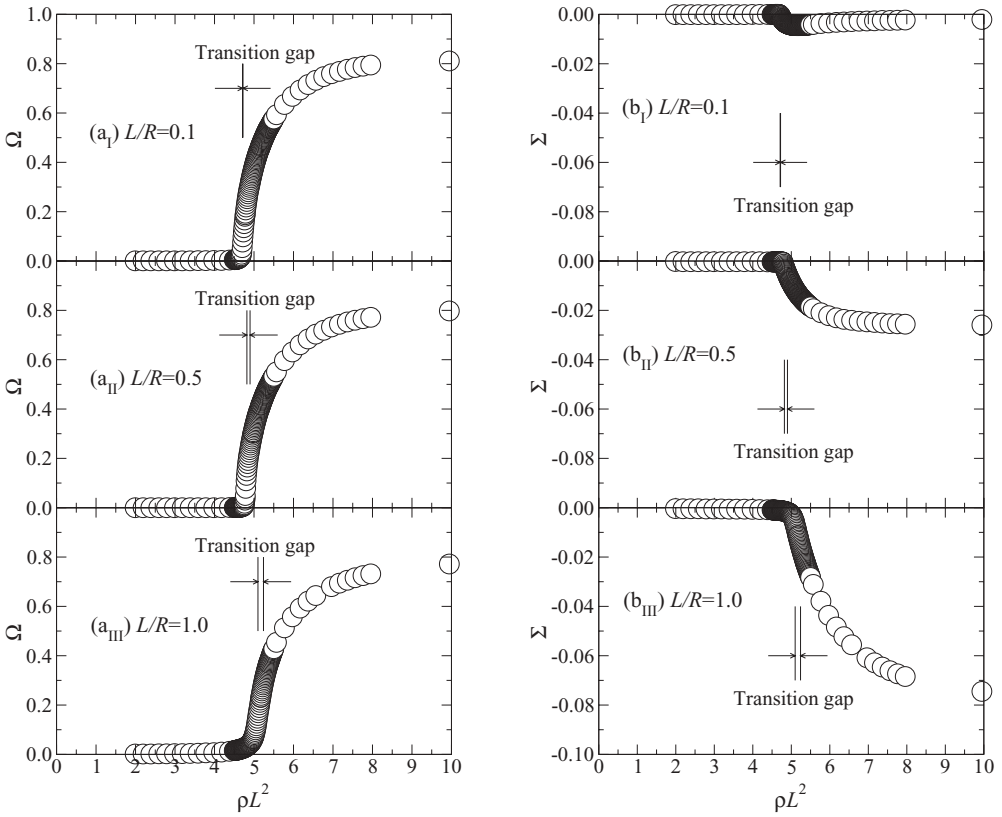

FIG. 5. Orientational and positional order parameters, Ω and Σ, plotted as functions of reduced density, ρL^2, for (a_I) and (b_I) $L/R = 0.1$, (a_{II}) and (b_{II}) $L/R = 0.5$, as well as (a_{III}) and (b_{III}) $L/R = 1.0$. Data points associated with nonzero Ω and Σ were produced from splay configurations. The area inside the two vertical lines indicates the transition region discussed in Sec. III F.

The global spatial order parameter,

$$\Sigma = \int P_2(\cos\Theta)\, f(\Theta,\Phi;\theta)\sin\Theta d\Theta d\Phi d\theta = \sqrt{\frac{8}{5}}\pi\phi_{200}, \tag{32}$$

yields a 0 value in the isotropic phase, a positive value in a spatially ordered state where the pole regions are more dense, and a negative value in a spatially ordered state where the equator region is more dense.

At a few selected L/R, Fig. 5 shows Ω and Σ as functions of ρL^2. The initial guess of $f(\Theta,\Phi;\theta)$ in the numerical search was taken from the optimized function determined earlier at a slightly higher value of ρL^2. This way, in the region where a disorder state is stable (reflected by significantly nonzero Ω and Σ), the minimized results closely adhered to a splay configuration. As ρL^2 is lowered passing a transition region, an isotropic state is reached in the low density region, where $\Omega = \Sigma = 0$. Comparing Σ of the case $L/R = 0.1$ with those of the systems, $L/R = 0.5$ and 1.0, we can also see that the spatial ordering is weakened as L/R becomes smaller. This is consistent with the expectation that our model system becomes spatially disordered approaching the asymptotic limit of a flat two-dimensional system, $L/R \ll 1$, while keeping an orientational order (a nematic state).

F. Isotropic-splay phase transition

To further study the characteristics of the isotropic-splay transition, we used splay-relevant, undetermined ϕ_{l0n} and substituted them into Eq. (24), to produce an expansion of the free energy. In comparison with the Landau expansion in the phase-transition theory, one important feature in our expansion is the existence of third-order terms coupling Ω with Σ and other ϕ_{l0n} factors. This can be understood from the symmetry of the problem without actually expanding the free energy. For example, making the transformation of $\Omega \to -\Omega$ implies the change from splay to latitudinal helicoidal or vice versa; these are two different physical states, hence the corresponding free energies cannot be identical. Moreover, the change in the free energies cannot be compensated by the transformation of other coefficients ϕ_{l0n}. An immediate implication is that in a Landau expansion odd-power terms exist, so that the associated phase transition is discontinuous. Using the numerical data presented above, we clarify the properties of the transition in this subsection.

The method used here is similar to the determination of the first-order isotropic-nematic phase transition in the lyotropic liquid-crystal theory, although there is no spatial disorder in the latter [13,14]. To determine the transition density, conceptually we consider two systems: one is in an isotropic phase with a number density $\rho_{\rm iso}$ and the other is in a splay state with $\rho_{\rm spl}$. These two systems are in phase equilibrium at the transition densities, in such a way that the chemical potentials,

$$\mu = (\partial F/\partial N)_A, \tag{33}$$

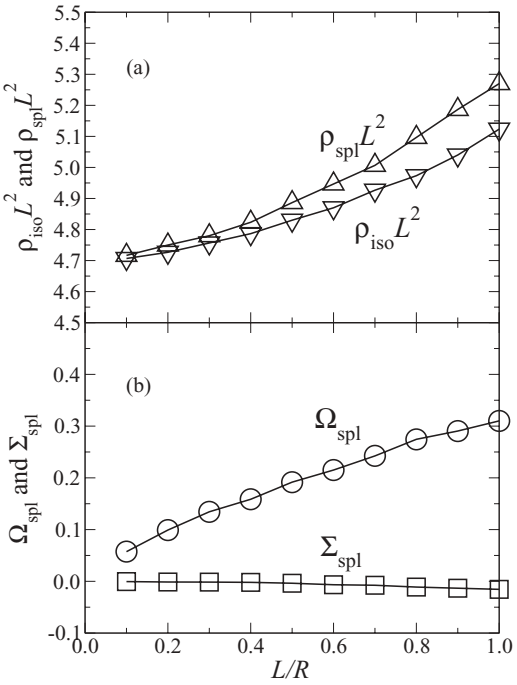

FIG. 6. (a) Transition densities $\rho_{iso}L^2$ (down triangles) and $\rho_{spl}L^2$ (up triangles) and (b) orientational and spatial order parameters, Ω and Σ, at $\rho_{spl}L^2$ plotted as functions of L/R.

are the same in the two systems. We also equate the osmotic pressures,

$$\Pi = (\mu N - F)/A, \tag{34}$$

in two systems, where $A = 4\pi R^2$ is the surface area,. The transition densities are determined from solving two nonlinear equations:

$$\mu_{iso}(\rho_{iso}) = \mu_{spl}(\rho_{spl}), \tag{35a}$$

$$\Pi_{iso}(\rho_{iso}) = \Pi_{spl}(\rho_{spl}). \tag{35b}$$

The free energy βF is already given in Eq. (22) for the splay branch and Eq. (23) for the isotropic branch. The derivatives of the free energy of the isotropic branch can be obtained analytically from Eq. (23), while those of the splay branch were obtained in this work by a numerical difference with respect to ρ.

The transition densities $\rho_{iso}L^2$ and $\rho_{spl}L^2$ are plotted in Fig. 6(a) by down and up triangles, respectively. The first-order transition gap is wider in larger L/R systems and converges to zero in the limit of a flat two-dimensional system ($L/R \to 0$). This fact implies that the first-order disorder-splay transition reduces to a continuous isotropic-nematic transition in flat two dimensions as $L/R \to 0$, within the validity of the Onsager model; the asymptotic reduced transition density at $L/R = 0$, 4.71, is consistent with the value found earlier, $\rho_c L^2 = 3\pi/2$ [21,39]. The first-order nature of the disorder-splay transition in finite L/R systems can be compared to the first-order nature of the isotropic-nematic transition in a three-dimensional lyotropic system [14,40–42].

Instead of the hypothetical phase-equilibrium physical picture, we are, however, dealing with a finite system where N (therefore ρL^2) is fixed. In a typical plot shown in Fig. 5 where ρ continually changes, we can divide ρ into three regions. In the $\rho \leqslant \rho_{iso}$ or $\rho \geqslant \rho_{spl}$ region, the system is either in a disorder or splay state. In the $\rho_{iso} < \rho < \rho_{spl}$ region, the system is actually in a crossover state between the disorder and splay states. Both Ω and Σ are different in this region from the splay branch plotted in Fig. 6(b). For an isotropic-nematic transition in the thermodynamic limit, this density region normally corresponds to a isotropic-nematic interface [26,27]. Because of the finite L/R ratio in the current model, such an interface cannot be clearly defined.

IV. CONCLUSIONS

In this paper, we demonstrated that the Onsager treatment for rigid rods can be generalized to study the system of curved rigid rods confined on the spherical surface. The excluded-volume interaction in the system can be approximated by a free-energy term that depends on both orientational and positional variables. We developed a numerical method which allows us to minimize the free energy within a controlled precision. We found that the free-energy minimum corresponds to a stable splay state and that the tennis-ball, rectangle, and cut-and-rotate splay configurations are all not stable, within a significantly wide parameter region searched computationally.

Experimentally accessible systems contain molecules that might have some degree of semiflexibility; the fact that $K_1 \sim K_3$ was estimated for 5CB molecules [20], a signal of the importance of molecular semiflexibility in influencing the splay and bend energy [37], makes it desirable to generalize the model presented in this paper to a semiflexible polymer system. The formalism is already available and was applied to the isotropic-nematic interface problem previously [27,43].

ACKNOWLEDGMENTS

The authors wish to thank the Natural Science and Engineering Council of Canada (NSERC) for financial support and the Shared Hierarchical Academic Research Computing Network (SHARCNET) for providing computational time.

[1] D. R. Nelson, Nano Lett. **2**, 1125 (2002).
[2] A. Fernández-Nieves, V. Vitelli, A. S. Utada, D. R. Link, M. Márquez, D. R. Nelson, and D. A. Weitz, Phys. Rev. Lett. **99**, 157801 (2007).
[3] T. Lopez-Leon, V. Koning, K. B. S. Davaiah, V. Vitelli, and A. Fernandez-Nieves, Nature Physics **7**, 391 (2011).
[4] K. M. Ho, C. T. Chan, and C. M. Soukoulis, Phys. Rev. Lett. **65**, 3152 (1990).
[5] A. Arsenault, S. Fournier-Bidoz, B. Hatton, H. Míguez, N. Tétreault, E. Vekris, S. Wong, S. M. Yang, V. Kitaev, and G. A. Ozin, J. Mater. Chem. **14**, 781 (2004).
[6] S. Mitragotri and J. Lahann, Nat. Mater. **8**, 15 (2009).

[7] F. Li, W. C. Yoo, M. B. Beernink, and A. Stein, J. Am. Chem. Soc. **131**, 18548 (2009).
[8] M. Mermin, in *Quantum Fluids and Solids*, edited by S. B. Trickey, E. D. Adams, and J. W. Dufty (Plenum Press, New York, 1977).
[9] T. C. Lubensky and J. Prost, J. Phys. II **2**, 371 (1992).
[10] V. Vitelli and D. R. Nelson, Phys. Rev. E **74**, 021711 (2006).
[11] M. Huber and H. Stark, Europhys. Lett. **69**, 125 (2005).
[12] S. Kralj, R. Rosso, and E. G. Virga, Soft Matter **7**, 670 (2011).
[13] L. Onsager, Ann. NY Acad. Sci. **51**, 627 (1949).
[14] T. Odijk, Macromolecules **19**, 2313 (1986).
[15] W.-Y. Zhang, Y. Jiang, and J. Z. Y. Chen, Phys. Rev. Lett. **108**, 057801 (2012).
[16] H. Shin, M. J. Bowick, and X. Xing, Phys. Rev. Lett. **101**, 037802 (2008).
[17] M. A. Bates, J. Chem. Phys. **128**, 104707 (2008).
[18] J. P. Straley, Phys. Rev. A **8**, 2181 (1973).
[19] A. Poniewierski and R. Hołyst, Phys. Rev. A **41**, 6871 (1990).
[20] J. D. Bunning, T. E. Faber, and P. L. Sherrell, J. Physique **42**, 1175 (1981).
[21] R. F. Kayser and H. J. Raveché, Phys. Rev. A **17**, 2067 (1978).
[22] R. Hołyst and A. Poniewierski, Phys. Rev. A **38**, 1527 (1988).
[23] B. G. Moore and W. E. McMullen, Phys. Rev. A **42**, 6042 (1990).
[24] W. E. McMullen, Phys. Rev. A **38**, 6384 (1988).
[25] H. Kimura and H. Nakano, J. Phys. Soc. Jpn. **55**, 4186 (1986).
[26] Z. Y. Chen and J. Noolandi, Phys. Rev. A **45**, 2389 (1992).
[27] Z. Y. Chen, Phys. Rev. E **47**, 3765 (1993).
[28] D. L. Koch and O. G. Harlen, Macromolecules **32**, 219 (1999).
[29] A. Poniewierski and R. Hołyst, Phys. Rev. A **38**, 3721 (1988).
[30] A. Poniewierski, Phys. Rev. E **47**, 3396 (1993).
[31] R. van Roij, M. Dijkstra, and R. Evans, J. Chem. Phys. **113**, 7689 (2000).
[32] See, e.g., G. B. Arfken, *Mathematical Methods for Physicists*, 2nd ed. (Academic Press, New York, 1972).
[33] See, e.g., R. L. Burden and J. D. Faires, *Numerial Analysis*, 8th ed. (Thomson Brooks, Belmont, 2005).
[34] See, e.g., R. Fletcher, *Practical Methods of Optimization*, 2nd ed. (Wiley, New York, 1987).
[35] See, e.g., P.-G. de Gennes, *The Physics of Liquid Crystals* (Clarendon, Oxford, 1974).
[36] D. R. Nelson and R. A. Pelcovits, Phys. Rev. B **16**, 2191 (1977).
[37] T. Sato and A. Teramoto, Macromolecules **29**, 4107 (1996).
[38] W.-Y. Zhang and J. Z. Y. Chen, Europhys. Lett. **94**, 43001 (2011).
[39] Z. Y. Chen, Phys. Rev. Lett. **71**, 93 (1993).
[40] A. R. Khokhlov and A. N. Semenov, Physica A **108**, 546 (1981).
[41] A. R. Khokhlov and A. N. Semenov, Physica A **112**, 605 (1982).
[42] Z. Y. Chen, Macromolecules **26**, 3419 (1993).
[43] Y. Jiang and J. Z. Y. Chen, Macromolecules **43**, 10668 (2010).